Proceedings of the 16th International Conference on Nuclear Engineering
ICONE16
May 11-15, 2008, Orlando, Florida, USA

ICONE16-48731

HIGH-CYCLE THERMAL FATIGUE IN MIXING TEES. LARGE-EDDY SIMULATIONS COMPARED TO A NEW VALIDATION EXPERIMENT

Johan Westin
Vattenfall Research and Development AB
SE-81426 Älvkarleby, Sweden

Pascal Veber, Lars Andersson
Onsala Ingenjörsbyrå AB
SE-43437 Kungsbacka, SWEDEN

Carsten 't Mannetje
Forsmarks Kraftgrupp AB
SE-74203 Östhammar, Sweden

Urban Andersson, Jan Eriksson, Mats Henriksson
Vattenfall Research and Development AB
SE-81426 Älvkarleby, Sweden

Farid Alavyoon
Forsmarks Kraftgrupp AB
SE-74203 Östhammar, Sweden

Claes Andersson
Ringhals AB
SE-43022 Väröbacka, Sweden

ABSTRACT

The present paper describes new experimental data of thermal mixing in a T-junction compared with results from Large-Eddy Simulations (LES) and Detached Eddy Simulations (DES). The experimental setup was designed in order to provide data suitable for validation of CFD-calculations. The data is obtained from temperature measurements with thermocouples located near the pipe wall, velocity measurements with Laser Doppler Velocimetry (LDV) as well as single-point concentration measurements with Laser Induced Fluorescence (LIF).

The LES showed good agreement with the experimental data also when fairly coarse computational meshes were used. However, grid refinement studies revealed a fairly strong sensitivity to the grid resolution, and a simulation using a fine mesh with nearly 10 million cells significantly improved the results in the entire flow domain. The sensitivity to different unsteady inlet boundary conditions was however small, which shows that the strong large-scale instabilities that are present in the mixing region are triggered independent of the applied inlet perturbations.

A shortcoming in the performed simulations is insufficient near-wall resolution, which resulted in poor predictions of the near-wall mean velocity profiles and the wall-shear stress. Simulations using DES improved the near-wall velocity predictions, but failed to predict the temperature fluctuations due to high levels of modeled turbulent viscosity that restrained the formation of small scale turbulence.

INTRODUCTION

High-cycle thermal fatigue in the vicinity of T-junctions (mixing Tees) is a potential cause of structural damages, which in some cases have resulted in leaks and power plant shut downs ([1],[2]). Although structural failures can be avoided by installation of static mixers or by regular replacement of components, it is necessary to identify the T-junctions that are at risk. For a detailed structural analysis, both the amplitudes and spectral distribution of the temperature fluctuations near the walls are needed which requires detailed knowledge of the flow field.

The flow in the T-junction is a challenging test case for Computational Fluid Dynamics (CFD), and the CFD-methods based on RANS (Reynolds Averaged Navier-Stokes equations) which are typically used in industrial applications have difficulties to provide accurate results for this flow situation. Recent studies using advanced scale-resolving methods such as LES and DES have shown promising results ([3]-[6]). However, detailed validation of the tools and methods is still required in order to determine their range of validity and their expected accuracy.

The present authors have in a previous study performed experiments and simulations on a T-junction geometry representative for a typical plant installation ([6]). The results were promising but also stressed the need for well-documented experimental data suitable for CFD-validation. The present

paper describes a new experimental and computational effort with the following objectives:

- Provide detailed experimental data on a generic test case of a T-junction suitable for CFD-validation.
- Perform Large-Eddy Simulations with a commercial software (Fluent), with focus on sensitivity studies regarding the influence of mesh resolution and inlet boundary conditions.

VALIDATION TEST CASE (EXPERIMENTAL DATA)

The model tests were carried out during 2006 at the Älvkarleby Laboratory, Vattenfall Research and Development. The test rig is illustrated in Figure 1, and was designed in order to obtain simple and well-defined inlet boundary conditions. The setup consists of a horizontal pipe with inner diameter 140 mm for the cold water flow (Q_2), and a vertically oriented pipe with inner diameter 100 mm for the hot water flow (Q_1). The hot water pipe is attached to the upper side of the horizontal cold water pipe. The length of the straight pipes upstream of the T-junction is more than 80 diameters for the cold water inlet, and approximately 20 diameters for the hot water inlet. A stagnation chamber with flow improving devices (tube bundles and perforated plates) is located at the entrance to each of the two inlet pipes. The origin of the coordinate system is in the centre of the T-junction, with the x-, y- and z-directions oriented along the horizontal main pipe, perpendicular to the main pipe and along the branch pipe respectively. The corresponding velocity components are denoted u, v and w.

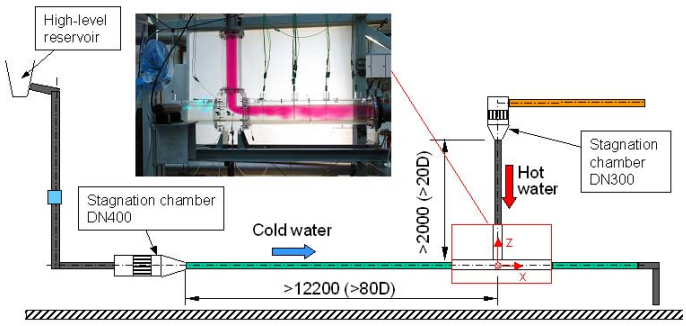

Figure 1 Side view of the test rig with a photo of the test section. Dimensions are in mm.

The temperature fluctuations near the walls were measured with thermocouples located approximately 1 mm from the pipe wall. Two different types of thermocouples were used, with an estimated frequency response of 30 Hz and 45 Hz respectively. Velocity profiles were measured with two-component Laser Doppler Velocimetry (LDV) in each inlet pipe as well as in cross-sections located 2.6 and 6.6 diameters downstream of the T-junction. The mixing process has also been studied with single-point Laser Induced Fluorescence (LIF) at isothermal conditions. The pipes near the T-junction were made of plexiglass tubes surrounded by rectangular boxes filled with water in order to reduce the diffraction when the laser beams pass the curved pipe walls.

The tests were carried out with a constant flow ratio $Q_2/Q_1=2$, which implies approximately equal flow velocities in the two inlet pipes. The temperature difference between the hot and cold water was 15°C, and the Reynolds number in both inlet pipes were approximately 10^5 for the test case considered in the present paper with bulk velocities of approximately 0.8 m/s. Tests were also carried out with the same flow ratio but varying Reynolds number (0.5×10^5 and 2×10^5) showing similar results.

As mentioned earlier the aim was to create a generic test case with well-defined inlet boundary conditions. The LDV-measurements in the cold water pipe just upstream of the T-junction showed mean velocity and turbulence profiles in good agreement with experimental data on fully developed pipe flow at similar Reynolds numbers (see e.g. ref. [7]). The length of the hot water inlet pipe was too short (20 diameters) to obtain fully developed flow conditions, but the inlet velocity profiles were measured and used in order to obtain inlet boundary conditions for the simulations.

When comparing computational and experimental results non-dimensional quantities are compared, such as

$$T^* = \frac{T - T_{cold}}{T_{hot} - T_{cold}}$$

$$\frac{T_{rms}}{\Delta T} = \frac{T_{rms}}{T_{hot} - T_{cold}}$$

in which ΔT is the temperature difference between the hot and cold water inlets $(T_{hot}-T_{cold})$. The normalization reduces the influence of small temperature variations between different test days. In the results part of the present paper the mean and fluctuating temperatures near the pipe walls are reported at the left, right, top and bottom side of the pipe, which are defined in Figure 2. Due to a mistake when assembling the T-junction, the thermocouples in cross sections x=2D, 4D, 6D and 8D are rotated 4° as compared to the design specifications, which must be taken into account when interpreting the data.

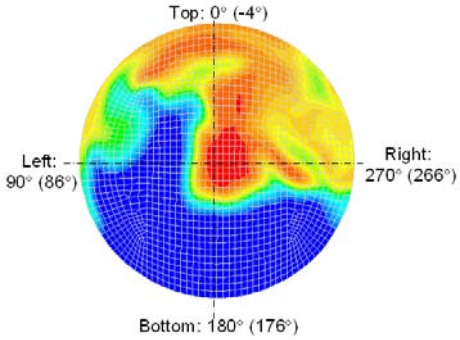

Figure 2 Illustration of left, right, top and bottom side of the pipe. Cross-section located at x=2D viewed in the streamwise direction. (Instantaneous temperatures from simulations with mesh 2).

During the course of the study it became clear that it was very difficult to perform laser measurements with temperature differences between the hot and cold water of $\Delta T \approx 15°C$, since the changes in the index of refraction deflected the laser beams. Thus, it was decided that the LDV- and LIF-measurements were carried out at isothermal conditions. The small changes in density and viscosity due to the temperature difference should have a negligible effect on the flow. However, in order to verify this assumption measurements were carried out both at isothermal conditions and with a temperature difference of 15°C at cross-sections in the hot inlet pipe and downstream of the T-junction at x/D=2.6. In both cross-sections the isothermal conditions gave almost identical results as obtained with a temperature difference between the two inlet flows.

The uncertainty in the mean temperature measurements with thermocouples is within ±0.5°C, which gives a constant uncertainty of 0.05 in terms of T*. Plots of T* and Trms are based on 45 minutes of data, which gives relatively small statistical uncertainties (typically less than 5% in Trms, except for a few locations near the bottom wall where the signal is highly intermittent). However, an additional uncertainty of 5% has been added to account for possible systematic errors. The total uncertainty in the temperature fluctuations is estimated to be 10% of the measured value, except near the bottom wall where an uncertainty of 15% has been assumed.

The uncertainty in the LDV-measurements is estimated to be between 6-8% for the different measured quantities, and the estimated uncertainty for the LIF-data is 10%. However, this value only applies to LIF-data that has been corrected for time variations in the inlet concentration.

COMPUTATIONAL MODEL

Mesh

Four different meshes have been used in the simulations of the T-junction (see Figure 3). Mesh 1 makes use of four boundary layer cells, and the wall-normal dimension of the first cell is only 0.3 mm in the pipe downstream of the T-junction. Mesh 1B is identical to mesh 1 except that the boundary layer cells are removed. The streamwise resolution is coarsened at a position x/D≈1.1, which can clearly be observed in Figure 3. The total number of cells in mesh 1 and 1B is approximately 0.5 million.

Mesh 2 consists of approximately 1 million cells and has a more uniform cell size distribution throughout the computational domain. This implies that the resolution near the T-junction is similar with mesh 1 and mesh 2, while the streamwise resolution upstream and downstream of the T-junction is higher in mesh 2. No boundary layer cells are used in mesh 2, and the wall-normal dimension of the first cell is approximately 2 mm. Another difference between mesh 1 and mesh 2 is the mesh design in the T-junction. Mesh 1 makes use of an O-type mesh that creates cells with a 45°-skew near the T-junction, while mesh 2 has a different mesh design with less skewed cells. Mesh 3 is designed similarly as mesh 2 but with a refined grid, resulting in almost 10 million cells.

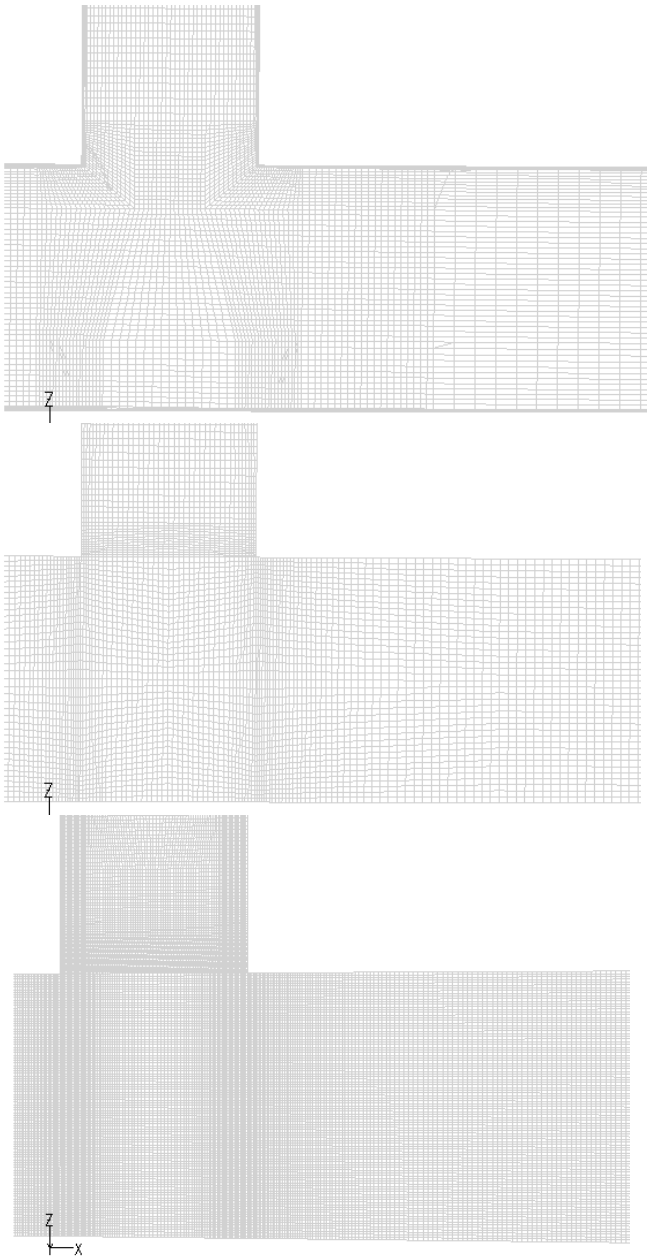

Figure 3 Mesh 1 (top), mesh 2 (middle) and mesh 3 (bottom). Cross section at y=0.

Numerical schemes

All Large Eddy Simulations reported in the present paper make use of the Wall-Adapting Local Eddy Viscosity (WALE) model. The WALE-model is a Smagorinsky-type model but with a modified dependence on the resolved strain field which is supposed to provide an improved near-wall behavior. Non-iterative time advancement (NITA) has been chosen for time control with a second order implicit scheme. The time step is

set to get a Courant number less than 1 in most of the model, so 1 ms for mesh 1, 0.8 ms for mesh 2 and 0.5 ms for mesh 3 is used. The Fractional Step algorithm has been used for the pressure-velocity coupling. For the pressure, the discretization scheme is Presto, for momentum, Bounded Central Difference and for energy, Quick.

One simulation was also carried out using Detached Eddy Simulations (DES) with the SST k-ω model. For more details on the models, see ref. [8].

Boundary conditions

All calculations make use if adiabatic walls and no-slip boundary conditions. The mean inlet velocity profile for the cold inlet is taken from a RANS-calculation based on a straight pipe with periodical boundary conditions, since the experimental data showed that the flow field is in good agreement with fully developed pipe flow. For the hot inlet, the mean velocity profile is taken from a RANS-calculation under development in order to fit the experimental profile.

Different unsteady inflow boundary conditions have been applied. First of all, simulations were carried out without any unsteady fluctuations applied at the two inlets ("no perturbation"). The second case makes use of the vortex method which is one of the methods implemented in Fluent [8]. A fluctuating (time dependent) vorticity field is added to the mean profiles described in the previous section. The vorticity field is two-dimensional in the plane normal to the streamwise direction, and the spatial distribution and the amplitude of the vortices are governed by the profiles of kinetic energy and dissipation rate obtained from RANS-calculations.

To have better control of the fluctuating velocities at the inlet boundaries a method using isotropic turbulence was applied (see ref. [9] for more details). The isotropic turbulence was scaled and added to the mean velocity profiles obtained from the RANS-calculations, and an instantaneous velocity field was generated for each time step. A file containing 12000 velocity fields (time steps) was generated for each inflow boundary and used as input during the simulation.

Performed simulations

Table 1 summarizes the main settings in the simulations of the T-junction. The sampling time (t_{samp}) denotes the length of the time sequence used in the data evaluation. Usually the simulation was carried out for approximately 4 seconds before the data sampling was started, which corresponds to at least two complete flow passages through the model.

Table 1 Performed simulations. All simulations except case T2iso-DES are made with LES using the WALE subgrid-scale model.

Case	Mesh ID	Mesh #cells	Δt (ms)	Q_2/Q_1	t_{samp} (s)	Unsteady BC
T1vm-FKA	1	0.52M	1.0	2.01	29.0	Vortex meth.
T1Bvm	1B	0.45M	-"-	2.01	21.8	-"-
T2vm	2	0.93M	0.8	1.93	19.6	-"-
T2np	2	-"-	-"-	-"-	27.0	No pert.
T2iso	2	-"-	-"-	-"-	13.5	Isotropic turb.
T2iso-DES	2	-"-	-"-	-"-	8.6	Isotropic turb.
T3vm	3	9.5M	0.5	-"-	8.3	Vortex meth.

RESULTS

Temperature data

Typical instantaneous temperature fields downstream of the T-junction are illustrated in Figure 4 for simulations with two different mesh resolution. As expected the fine mesh generates more small-scale structures. Quantitative comparisons between experimental data and simulations with different mesh resolution are given in Figure 5 and Figure 6, showing the non-dimensional mean and fluctuating temperatures near the pipe wall at the top, bottom, left and right side of the pipe. The overall agreement between simulations and experiments is good, and considerably better than obtained in refs. [5]-[6] that were based on a previous experimental study. It should also be taken into account that some of the simulation data suffer from a limited sampling time. For example the fluctuations near the bottom wall close to the T-junction originates from a few isolated "spikes" of hot water reaching the bottom wall, and especially for case T3vm the data set is too short to obtain statistically accurate results at this position.

The main discrepancy between simulations and experimental data can be seen in the temperature fluctuations at the left and right side of the pipe at x/D=2. A significant difference between cases T2vm and T1vm-FKA is that the cell size near the wall is much smaller in the latter case despite the fact that the total number of cells is larger in case T2vm. In case T2vm the wall-normal dimension of the first cell is approximately 2 mm, with only 0.3 mm in case T1vm-FKA. The temperature fluctuations at x/D=2 were considerably smaller in case T1vm-FKA and closer to the experimental data than in case T2vm. When the boundary layer was removed (cf. case T1Bvm), the temperature fluctuations increased close to the values obtained in case T2vm. The best overall agreement, however, was obtained with case T3vm, i.e. the simulation with the finest mesh in the bulk flow. It should be noted that three different subgrid-scale models (WALE, Standard Smagorinsky and Dynamic kinetic energy model) were compared during

initial tests with the coarse mesh (Mesh 1), and all of them showed similar results regarding the temperature fluctuations at the left and right pipe wall at x/D=2.

Figure 7 shows spectra of the temperature fluctuations near the left pipe wall. Also in this graph the agreement between simulations and experiments is good. As previously discussed, case T1vm-FKA has a very fine mesh near the wall, but a coarser mesh in the bulk flow as compared to cases T2vm and T3vm. Figure 7 shows that the spectral distribution of the temperature fluctuations near the wall is mainly dependent on the mesh resolution in the bulk flow, and the spectra obtained for cases T2vm and T3vm contain energy at higher frequencies than in case T1vm-FKA.

It should be stressed that the results in Figure 7 shows considerably better agreement with experimental data than obtained in refs. [5] and [6]. Those simulations were based on a different experimental study, and the simulation results always predicted energy at higher frequencies than observed in the experiment.

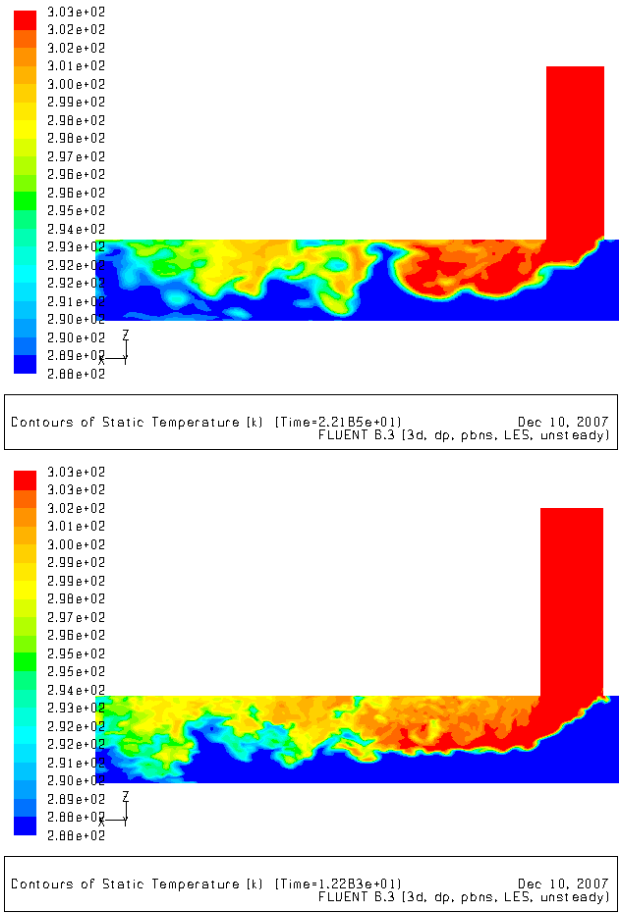

Figure 4 Instantaneous temperature fields at y/D=0 with different computational mesh. Case T2vm (top figure) and case T3vm (bottom figure).

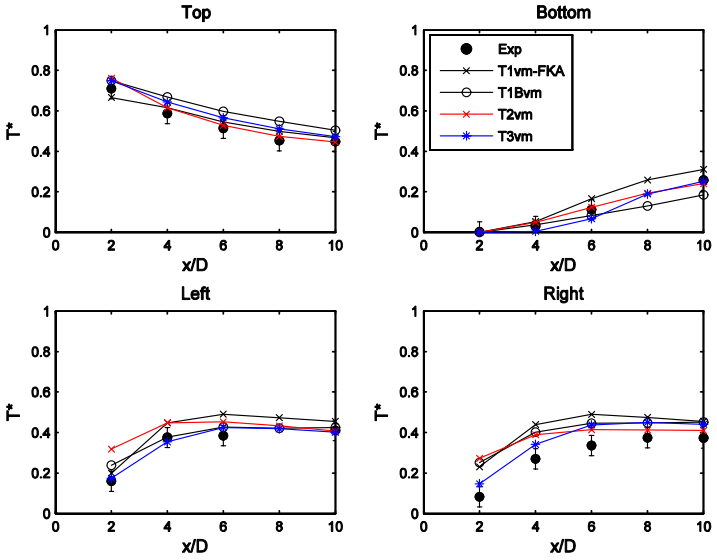

Figure 5 Non-dimensional mean temperatures near the wall obtained with different computational mesh. The four plots correspond to the top, bottom, left and right side of the pipe.

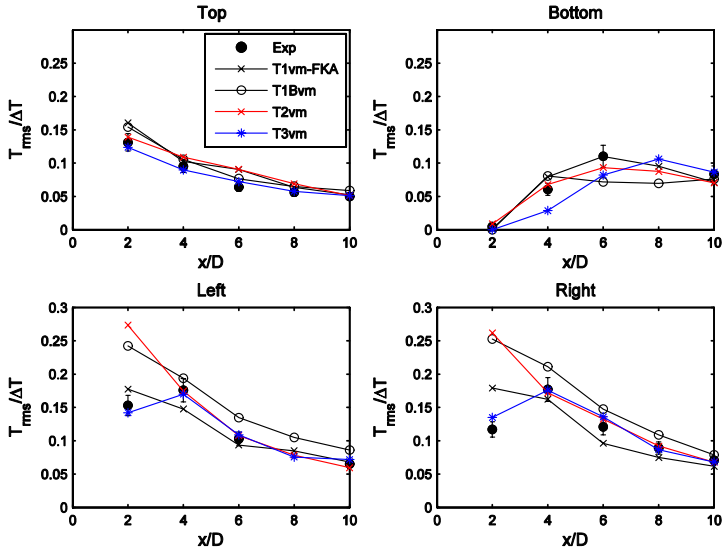

Figure 6 Non-dimensional temperature fluctuations near the wall obtained with different computational mesh.

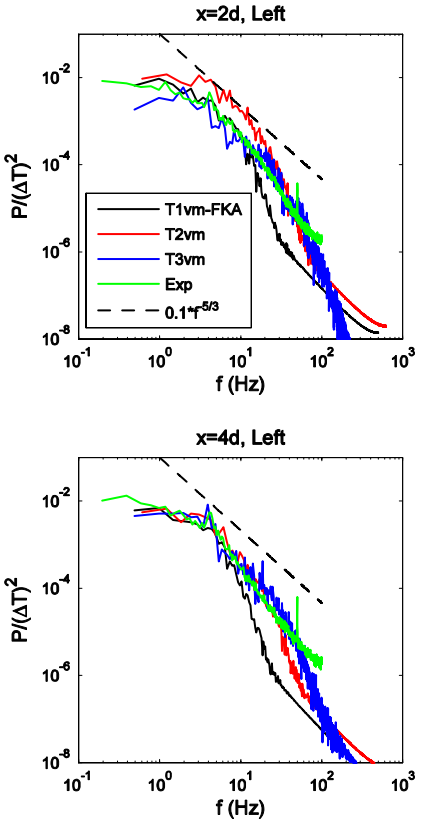

Figure 7 Spectra of temperature fluctuations 1 mm from the pipe wall at the left side of the pipe at streamwise positions x/D=2 (top figure) and x/D=4 (bottom figure).

Velocity data, centerline

The computed fluctuating velocities (resolved scales) along the centerline of the pipe are shown in Figure 8 together with data from the LDV-measurements. The finest mesh (case T3vm) gives almost perfect agreement with the experimental data, but also the results with a coarser mesh (cases T1vm-FKA and T2vm) follow the experimental data quite well. As mentioned before, mesh 1 is significantly coarsened in the streamwise direction at the position x/D=1.1. This implies that the filter length in the LES is suddenly increased, which affects the prediction of the turbulent fluctuations. This can be observed as a "kink" in the w_{rms}-curve at x/D=1.1.

Turbulence spectra near the centerline at x/D=2.6 are displayed in Figure 9 for the u- and v-component. The increased spectral resolution with the fine mesh used in case T3vm is evident. However, the maximum energy containing frequencies in all simulations are lower than estimated from the computational mesh and the bulk velocity. In case T1vm-FKA the spectral energy is quickly reduced above 20-30 Hz, and for case T3vm the energy drops off at about 80 Hz.

It is worth noticing that the spectra for the v-component contain a relatively distinct peak at 3-4 Hz. This peak can be associated with a spanwise oscillation similar to the vortex shedding downstream of a cylinder. The v-component was not measured with the two-component LDV, but the spanwise oscillations could be observed both in the flow visualizations as well as in some of the temperature measurements near the wall (see e.g. the measured spectrum near the left wall at x/D=4 in Figure 7).

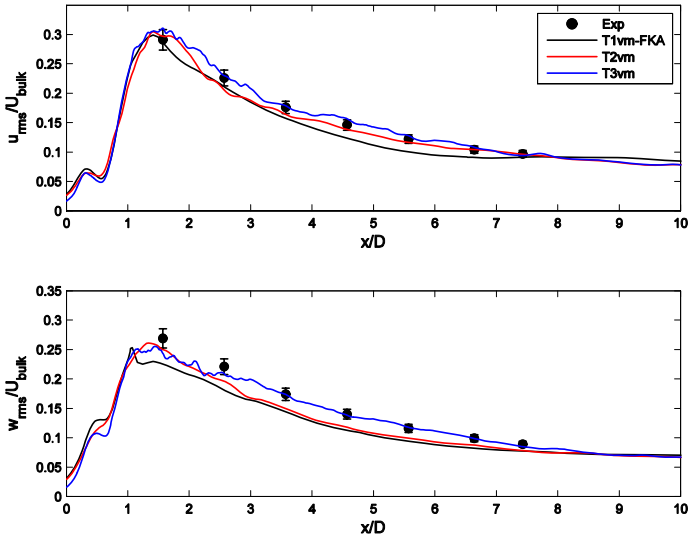

Figure 8 Development of the velocity fluctuations (u- and w-component) along the centerline of the pipe.

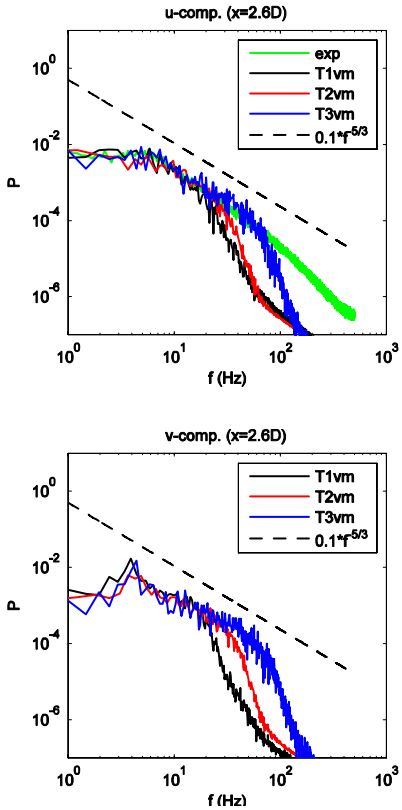

Figure 9 Turbulence spectra (u- and v-component) at the centerline of the pipe at x/D=2.6.

Velocity data, x/D=2.6

Mean velocity profiles obtained from the simulations are compared to experimental data in Figure 10 for the cross-section x/D=2.6. Especially for the case T3vm the sampling time for the statistical evaluation is quite short (8.3 s), which implies that the profiles are not particularly smooth. However, the agreement between case T3vm and the experimentally obtained mean velocity profiles is very good, and it is worth noticing that even the very small W-velocity is predicted correctly in this simulation. Also the simulations with coarser mesh capture the main characteristics of the experimental data.

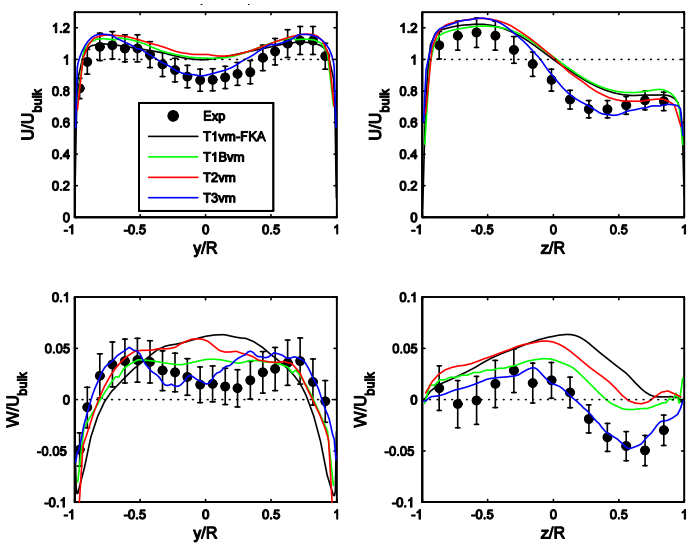

Figure 10 Mean velocities at x/D=2.6. Left and right columns show profiles measured along the y-axis and the z-axis respectively.

The corresponding Reynolds-stresses at position x/D=2.6 are presented in Figure 11. Again, the agreement between experimental data and case T3vm is remarkable. However, also the coarser mesh simulations provide results that in many cases can be considered as adequate, although the fluctuation levels are underpredicted as compared to the experiments.

The influence of the computational mesh on the flow field is further illustrated in Figure 12, showing in-plane mean velocity vectors at cross-section x/D=2. The flow is quite modified with the finer mesh, and the secondary vortices are better defined for case T3vm. It should be emphasized that the velocity vectors in Figure 12 are based on time-averaged velocities, which means that more distinct secondary flows may not necessarily imply more efficient thermal mixing. However, previous studies (e.g. refs. [5] and [6]) showed the importance of a correct prediction of the secondary flows originating from an upstream bend in order to predict the temperature fluctuations in the T-junction. In the present case there are no upstream bends that can create secondary flows, but the smaller diameter hot water jet will act as an obstacle for the cold water flow in the main pipe. It can be anticipated that the flow field downstream of the T-junction will include two symmetrical counter-rotating vortices trying to recover the momentum loss downstream of the obstacle.

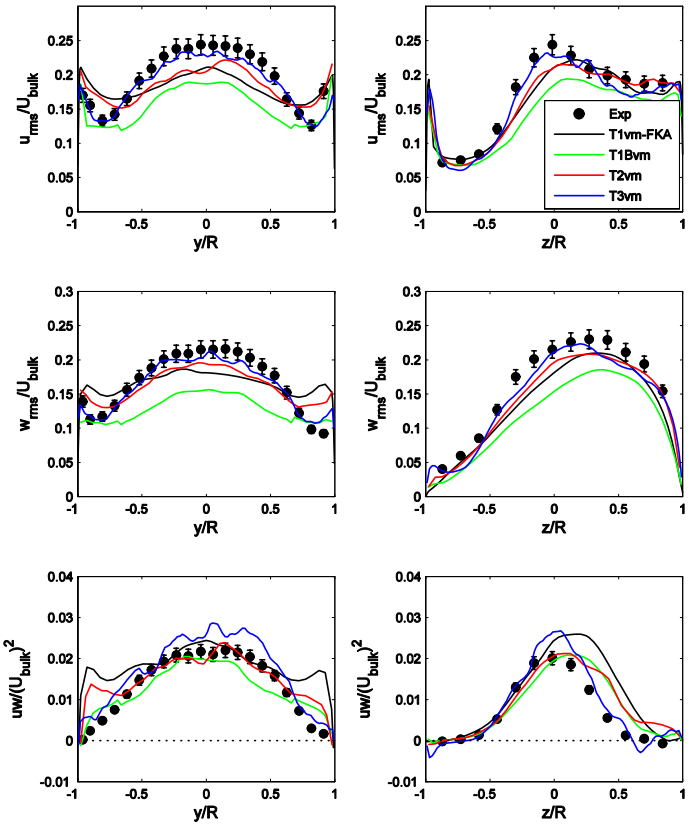

Figure 11 Velocity fluctuations (rms) and Reynolds shear stresses at x/D=2.6. Left and right columns show profiles measured along the y-axis and the z-axis respectively.

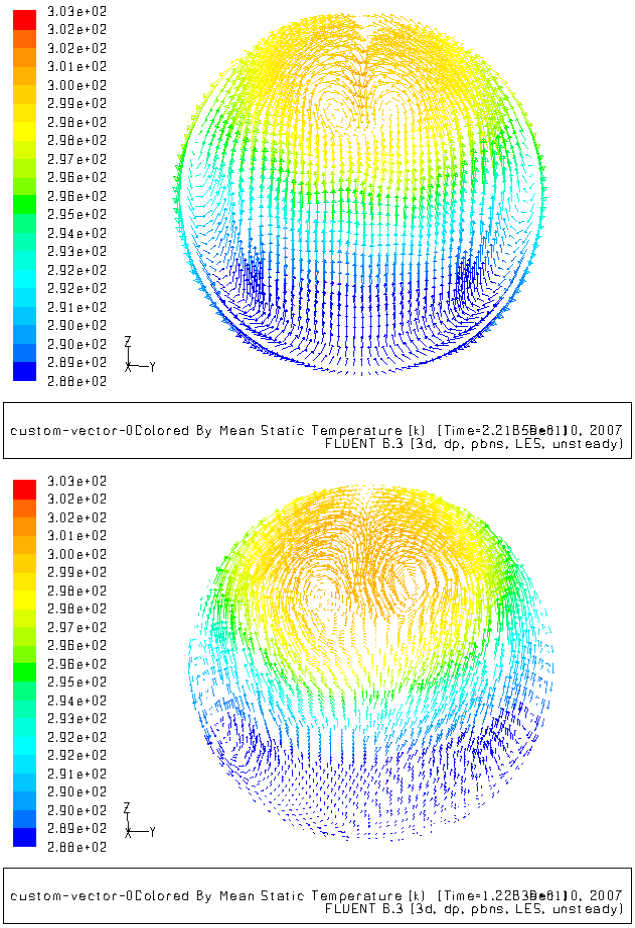

Figure 12 In-plane mean velocity vectors coloured by mean temperatures in cross-section x/D=2 for case T2vm (upper) and case T3vm (lower).

Velocity data, x/D=6.6

The mean velocity and Reynolds stress profiles at position x/D=6.6 are shown in Figure 13. At this position most of the profiles have become nearly symmetric with respect to the pipe axis, and the turbulence fluctuations (u_{rms} and w_{rms}) show almost equal and constant values over the entire cross section. A small asymmetry in the z-direction can be discerned in the w_{rms}- and the uw-profiles (not shown), which are the only remaining signs of the upstream wake created by the hot water jet. The results obtained from the simulations with different computational grids are all in good agreement with the experimental data.

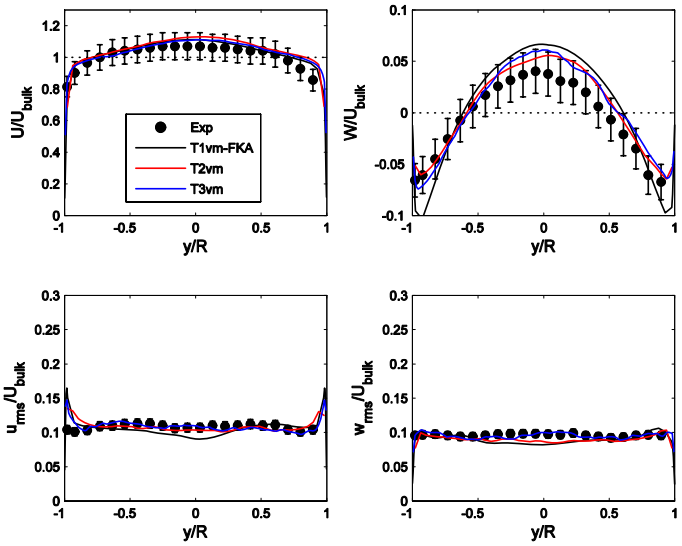

Figure 13 Mean velocity and rms-profiles at x/D=6.6 measured along the y-axis.

Turbulent kinetic energy

Figure 14 shows turbulent kinetic energy based on the simulated resolved turbulence in case T1vm-FKA. The abrupt increase in the cell size at x/D≈1.1 can be observed in the kinetic energy field. By increasing the cell size the filter length used in the LES is changed accordingly, resulting in a sudden reduction of the resolved turbulent kinetic energy. A comparison between the coarse and the fine mesh simulations revealed a stronger turbulence production in the shear layer originating from the left corner of the T-junction when a fine mesh is used.

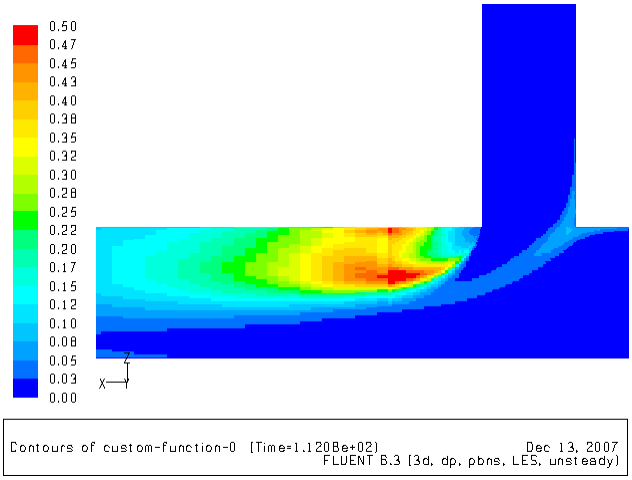

Figure 14 Turbulent kinetic energy at y=0 case T1vm-FKA.

Concentration/temperature data

The experimental study also included concentration measurements with single-point Laser Induced Fluorescence (LIF). The measurements were carried out at isothermal conditions (i.e. equal temperatures in the main and the branch pipe), but with a fluorescent dye added to the cold water flow. Since the temperature difference between hot and cold water ($\Delta T=15°C$) is small in the simulated test case, a comparison between the isothermal concentration measurements and the simulated temperature field is expected to be relevant. The non-dimensional quantity $C^*=1- C/C_{100}$ is plotted and compared to the simulated temperatures, where C_{100} corresponds to the concentration of fluorescent dye in the cold water flow.

During the course of the experimental study it was learned that a continuous correction for variations in the inlet concentration is necessary in order to achieve accurate data. Such correction was carried out for the measurements at x/D=6.6 (Figure 15), which shows quite good agreement between experiments and simulations both regarding mean and fluctuating temperatures. LIF-measurements were also carried out at x/D=2.6 (not shown), but since no concentration correction was carried out the experimental uncertainty in the data is significant and difficult to quantify. However, the discrepancies between the uncorrected data and the simulation results were large at this cross-section.

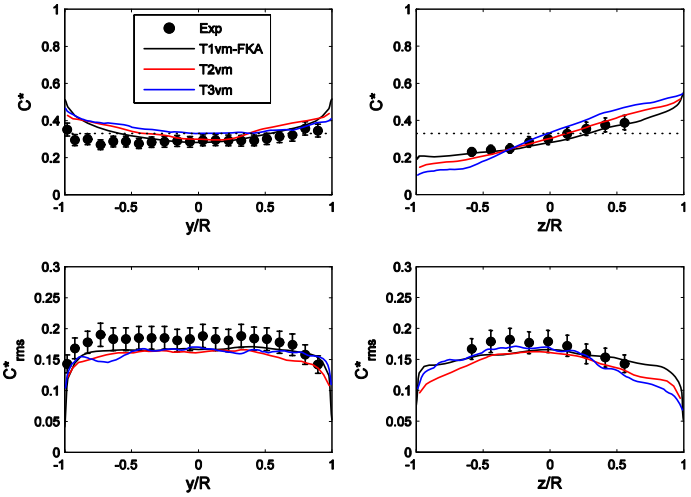

Figure 15 Measured concentration data (mean and rms) compared with predicted mean and fluctuating temperatures at x/D=6.6. Left and right columns show profiles measured along the y-axis and the z-axis respectively. The dotted lines show C*=0.33.

Different turbulence inlet boundary conditions

One objective of the present study was to investigate the influence of different unsteady inlet boundary conditions. Besides the vortex method that is implemented in Fluent, also simulations without any unsteady perturbations, as well as isotropic inlet turbulence read from an input data file, were tested. All simulations were conducted using mesh 2. The overall impression is that the inlet boundary conditions play a minor role for the simulated temperature fluctuations near the wall, and even without any perturbations at the inlet boundaries the mixing process is fairly well predicted. Close to the T-junction some differences can be observed, and in all cases the temperature fluctuations were overpredicted at x/D=2. This, however, is due to the coarse near-wall mesh. The fairly small sensitivity to the inlet boundary condition can most likely be explained by the fact that a strong shear layer instability is present in the T-junction, and the instability is triggered even without any inlet perturbations.

Comparison LES and DES

In all simulations performed in the present study the grid resolution is not sufficient in order to resolve the turbulence near the pipe walls. Even if Fluent automatically makes use of the law-of-the-wall when the near-wall grid resolution is insufficient, the predicted mean velocity profiles and the wall shear stress upstream of the T-junction differ significantly from typical pipe flow values. For this reason it was decided to make a calculation with a DES-model, which can be expected to provide better near-wall predictions. The main objective is thus to determine if the upstream velocity profile can influence the mixing downstream of the T-junction. Also, it is of interest to compare the influence of the subgrid-scale model used with the DES, which is different from the WALE-model used in the LES-calculations. The LES and DES turbulence models are run on mesh 2 and the results are presented in Figure 16-Figure 18. The two simulations make use of identical inlet boundary conditions due to the fact that the inlet perturbations are provided from an external input data file with isotropic turbulence.

The DES SST k-ω model is using a turbulence model that acts as an unsteady RANS (URANS) model in the part of the mesh where the turbulent length scale is smaller than the maximum grid spacing, and as a LES subgrid-scale model in the rest of the domain. As shown in Figure 16, upstream of the T-junction most of the domain is treated with the URANS solution, and the mean velocity profile agrees better with the experimental data as compared to the LES cases (not shown).

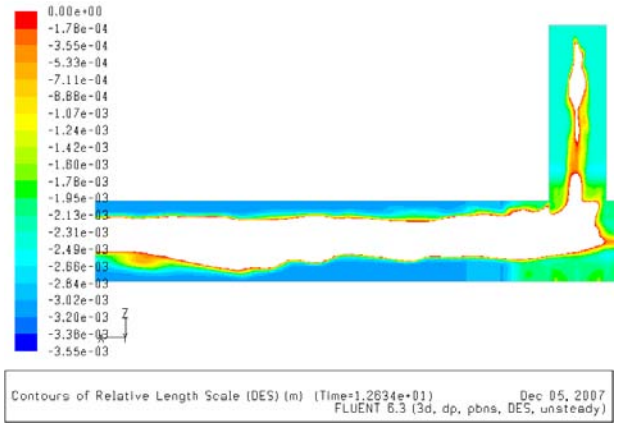

Figure 16 Contours of relative length scale in the DES. Negative values correspond to the so-called RANS-region, and the white region corresponds to the LES-region.

The non-dimensional mean temperatures presented in Figure 17 show a better agreement for the DES model, but the temperature fluctuations are too high with the DES model, although it has to be noted that the shape of the fluctuations at the left and right side is in better agreement with the experiment and with a less severe overprediction of the fluctuation level at x/D=2 as compared to the LES. However, the temperature signals obtained in the DES-simulation differ significantly from the LES, as can be observed in Figure 18. It is obvious that the DES-signal contains less energy at high frequencies, and the signal is dominated by low-frequency fluctuations with an amplitude that spans the entire temperature range between the hot and cold water inlet temperatures.

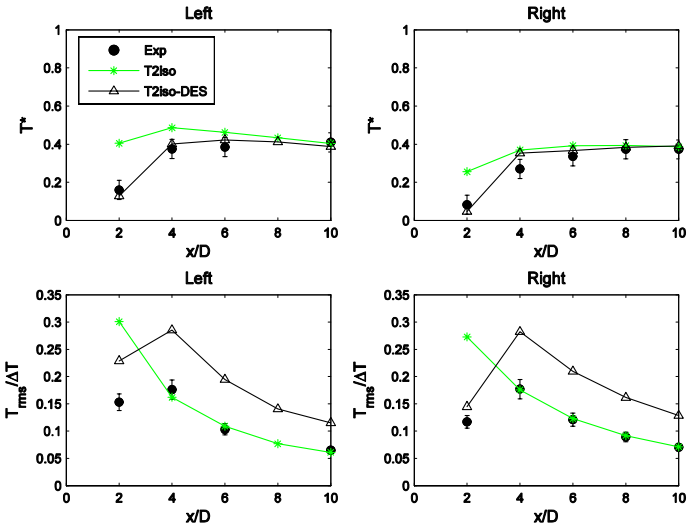

Figure 17 Non-dimensional mean and fluctuating temperatures near the left and right pipe wall obtained with LES and DES. Mesh 2, inlet-BC based on isotropic turbulence.

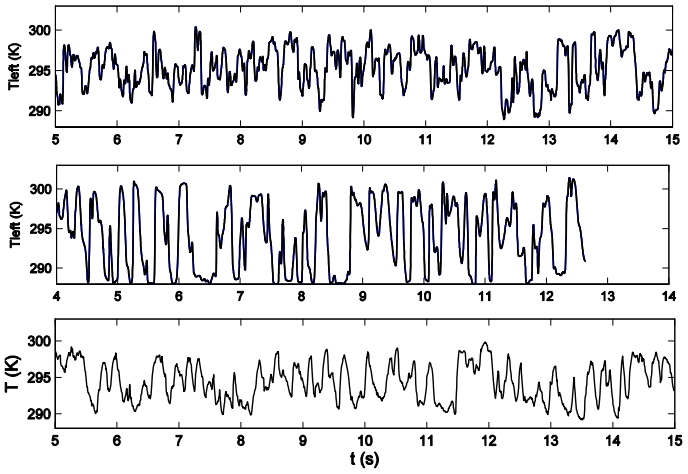

Figure 18 Temperature signals near the wall obtained with LES (top), DES (middle) and experimental data (bottom). Mesh 2, inlet-BC based on isotropic turbulence.

The present DES-model is significantly more dissipative (viscous) than the WALE-model, which can be ascribed to a larger quantity of modeled turbulent viscosity in the DES-case. This may be due to the large part of the domain in which the DES-model acts as an URANS-model, and even downstream of the T-junction only a limited central part of the bulk flow is treated as a LES-region. The DES is thus producing more modeled turbulence viscosity in certain regions that will be transported to the rest of the domain and restrain the formation of small resolved structures. The lack of small scales prevents an efficient thermal mixing, and the large temperature fluctuations that are observed with DES (cf. Figure 18) can be associated with the remaining large-scale motion of hot and cold fluid.

CONCLUDING REMARKS

Prediction of thermal mixing in a T-junction is a challenging test case for CFD, and advanced scale-resolving methods are required in order to simulate the flow field. To validate and assess such methods detailed experimental data are needed, and the present paper describes a new experimental study with the objective of providing well-documented boundary conditions and data suitable for validation. Computations using LES and DES have also been performed and compared with the experimental data.

The computational results were in qualitative good agreement with experimental data also when fairly coarse computational meshes were used, and the sensitivity to different unsteady inlet boundary conditions was small. These observations show that the strong large-scale instabilities that are present in the mixing region are triggered independent of the applied inlet perturbations and with fairly coarse mesh resolution. However, it was also shown that the predicted flow field could be significantly improved in the entire flow domain if the grid was refined.

The largest simulation with almost 10 million computational cells gave very good agreement between measured turbulence and temperature fluctuations. However, also in this case the near-wall resolution was insufficient leading to poor predictions of the near-wall mean velocity profiles and the wall-shear stress in the two inlet pipes. The present test case seems to be quite forgiving to this shortcoming and the predicted temperature fluctuations downstream of the T-junction were in good agreement with the experimental data. The difficulty of using LES for wall-bounded flows is well-known and should be kept in mind. It also emphasizes the need for alternative near-wall methods (hybrid methods) in order to use LES as a tool for industrial applications.

ACKNOWLEDGEMENTS

Fredrik Carlsson and Lars Davidson have provided valuable comments during the course of the present study, and Lars Davidson is also acknowledged for providing data files with isotropic turbulence. The work has been financed by Vattenfall Group functions, Forsmarks Kraftgrupp AB and Ringhals AB.

REFERENCES

[1] Faidy, C. (2002) High Cycle Thermal Fatigue: Lessons Learned From Civeaux Event. 2nd International Conference on Fatigue of Reactor Components, Snowbird, Utah.

[2] Chapuliot, S., Gourdin, C., Payen, T., Magnaud, J.P., and Monavon, A. (2005) Hydro-thermal-mechanical analysis of thermal fatigue in a mixing tee, *Nucl. Eng. Des.*, **235**, 575-596.

[3] Ohtsuka, M., Kawamura, T, Fukuda, T., Moriya, S., Shiina, K., Kurosaki, M., Minami, Y. and Madarame, H. (2003) LES analysis of fluid temperature fluctuations in a mixing Tee pipe with the same diameters, ICONE 11-36064, 11th International Conference on Nuclear Engineering, Tokyo, Japan, April 20-23, 2003.

[4] Braillard, O., Jarny, Y. and Balmigere, G. (2005) Thermal load determination in the mixing Tee impacted by a turbulent flow generated by two fluids at large gap of temperature, ICONE13-50361, 13th International Conference on Nuclear Engineering, Beijing, China, May 16-20, 2005.

[5] Veber, P. and Andersson, L. (2004) CFD calculation of flow and thermal mixing in a T-junction – time dependent calculation – Part 2. Teknisk not 2004/21 Rev 0. Onsala Ingenjörsbyrå AB.

[6] Westin, J., Alavyoon, F., Andersson, L., Veber, P., Henriksson, M. and Andersson, C. (2006) Experiments and unsteady CFD-calculations of thermal mixing in a T-junction, CFD4NRS, Garching, Germany.

[7] Zagarola, M.V. and Smits, A.J. (1998) Mean-flow scaling of turbulent pipe flow, *J. Fluid Mech.*, **383**, 33-79.

[8] Fluent version 6.3.26, documentation

[9] Davidson, L. (2007) Using synthetic fluctuations as inlet boundary conditions for unsteady simulations, Advances and Applications in Fluid Mechanics, vol. 1, no. 1, pp. 1-35.